PAPER

Check for updates

Effect of heat treatment under vacuum on structure and visible-light photocatalytic activity of nano-TiO$_2$

Zhengyuan Gao,[a] Pengfei Sun,[a] Yiliu Fang,[a] Chuanqiang Li, [iD] *[b] Xiaoya Yuan,[b] Xuxu Zheng[ab] and Jiacheng Gao[c]

Nano-TiO$_2$ is known as a photocatalyst with high catalytic activity. However, it should be emphasized that the bandgap of nano-TiO$_2$ is wide, which limits its photocatalytic efficiency in response to visible light and thus hinders its potential application. Improving the photocatalytic activity of nano-TiO$_2$ under visible light by the strategy of heat treatment under vacuum was investigated in this study. The structure and photocatalytic activity of nano-TiO$_2$ before and after heat treatment under vacuum were compared and analyzed by XRD, TEM, HRTEM, XPS and UV-Vis-NIR, respectively. The results show that oxygen vacancies were introduced into the crystal structure of nano-TiO$_2$ to change its inherent energy band structure. Particularly, the samples after heat treatment under vacuum exhibited high photocatalytic activity under visible light. In addition, the formation mechanism of non-stoichiometric compound TiO$_{2-x}$ and the mechanism of oxygen vacancy defects to expand the wavelength of light that nano-TiO$_2$ absorbs to the visible portion of the spectrum have also been addressed in this paper.

Introduction

The discovery made by Fujishima and Honda in 1972 indicated that water and other substances could be decomposed by a TiO$_2$ single-crystal electrode under visible light.[1] This finding provided a new application field for TiO$_2$ based photocatalysts. In recent years, the research on photocatalysis technology of TiO$_2$ has attracted increasing attention from scientific communities due to its appealing advantages such as the high catalytic oxidation activity, the fast photocatalysis degradation reaction, the high photocatalytic activity, and so on.[2,3] Thus, TiO$_2$ based photocatalysts have great potential for applications in a wide range of areas, for example, environmental management,[4] development of new energy,[5–9] air purification,[10,11] sewage treatment,[12] self-cleaning ceramics,[13,14] sterilization material,[15–18] photoelectric conversion,[19,20] *etc.* However, the application of TiO$_2$ based photocatalysts is still limited due to the following two aspects. Firstly, the wide band gap of TiO$_2$ limits its photocatalytic efficiency in response to solar radiation (only UV light, accounting for ∼5% of the solar spectrum can be utilized).[21] Secondly, it is easy for photoinduced electron hole pairs to recombine, leading to low photocatalytic performance

and then low rate of degradation to contaminants. To this end, considerable efforts have been made to improve the photocatalytic efficiency of TiO$_2$ in response to visible light. The existing methods mainly include doping,[22–29] compound semiconductor,[30] noble metal deposition,[31] dye sensitization,[32] and surface pretreatment by introducing structural defects.[33–35] The crystal structure and band structure of nano-TiO$_2$ could be changed upon using ion doping by ion implantation and chemical doping, and also the photocatalytic activity of TiO$_2$ can be improved by the methods of dye sensitization or compound semiconductor. However, those methods have many disadvantages, for example, the thermal stability is poor, the doped ion is easy to become the composite center of electron hole pairs, and the optical absorption efficiency is low.[36] It is thus highly desired to develop an effective method to improve the photocatalytic efficiency of TiO$_2$ in response to visible light, but not with the drawbacks inherent in the aforementioned existing methods. The effort in this paper is to provide an effective solution to such problem.

Of particular interest in this paper is to improve the photocatalytic efficiency of TiO$_2$ in response to visible light by heat treatment in vacuum. On the basis of non-stoichiometric compounds, we tried to introduce the oxygen vacancy into the crystal structure of nano-TiO$_2$ to change its inherent energy band structure. As a result, it can absorb visible light over a certain range of wavelength. In addition, we also investigated the mechanism of photocatalytic activity under visible light on the basis of lattice imperfections and energy band of semiconductor to propose a modified technology that is effective to

[a]School of Mechatronics and Automotive Engineering, Chongqing Jiaotong University, Chongqing, China, 400074

[b]School of Materials Science and Engineering, Chongqing Jiaotong University, Chongqing, China, 400074. E-mail: lichuanqiang_cn@163.com

[c]School of Materials Science and Engineering, Chongqing University, Chongqing, China, 400044

improve the photocatalytic efficiency of TiO_2 in response to visible light.

Experimental

To study the effect of heat treatment in vacuum on structure and photocatalytic activity of nano-TiO_2 under visible light, the nano-TiO_2 anatase powders (MTI, ~6.40 nm in size, 99.99% purity) was taken as the test subjects. The TiO_2 (0.5 g) nano-particles were placed into corundum crucible to be annealed in VSFV-30 type vacuum furnace. Heat treatment temperatures in this process were taken as 400 °C and 1000 °C, respectively, with a holding time of 40 min. The samples were naturally cooled to room temperature in furnace. Before the TiO_2 nanoparticles were heated, the vacuum furnace was pumped below the degree of ~1.0×10^{-1} Pa. During the whole heating, heat preservation, and cooling process, the vacuum of furnace was maintained at ~1.0×10^{-1} Pa by pumping vacuum continuously. Then the samples of TiO_2 nanoparticles was taken out until the temperature is cooled to room temperature.

The phase purity of the samples was verified by powder X-ray diffraction (PXRD) (Bruker D8 ADVANCE AXS) using CuKα radiation ($\lambda = 1.5418$ Å) in the range $2\theta = 10$–90°. The size and crystal structure of TiO_2 samples analyzed using transmission electron microscopy (TEM) (Tecnai G2 F20) at an acceleration voltage of 200 kV. Future analysis was carried out using high-resolution X-ray photoelectron spectroscopy (XPS) (Gammadata-Scienta SES 2002) and UV-Vis-NIR Spectropho-tometer (Model UV-3101PC Shimadzu) with wavelength ranging from 200 to 700 nm.

The photocatalytic performance of the catalysts were assessed by photo-degradation of methyl orange (MO) solution under visible light. All the experiments were carried out using a BILON-CHX-V photoreactor (Shanghai Bilon Instruments Manufacture Co., Ltd., Shanghai, China) and a 500 W xenon lamp with working current 5 A. The intensity of irradiation was 100 mW cm^{-2} 5 mg of catalysts were mixed with 40 mL of MO solution (20 mg L^{-1}) and kept stirring in the dark for 1 h to establish the adsorption equilibrium. During the irradiation, 3 mL of the reaction solution was withdrawn at certain time intervals and centrifuged to remove the catalysts. The decolor-ization efficiency was determined by the concentration of MO studied by the spectrophotometer (AOE, Shanghai, China) at the maximum absorption wavelength of 464 nm.[37–39] The degradation rate was calculated by the following formula: degradation rate (%) = $100 \times (C_0 - C_t)/C_0$. Where C_0 is the initial concentration of MO (mg L^{-1}); C_t is the concentration of MO in another given irradiation time (mg L^{-1}).

Results and discussion

The effects of heat treatment in vacuum on structure of nano-TiO_2

The XRD pattern of nano-TiO_2 after treatment in vacuum is represented in Fig. 1. Analysis of testing results shows that the structure of TiO_2 nanoparticles still belongs to anatase after heat treatment in vacuum at 400 °C, with the grain size being
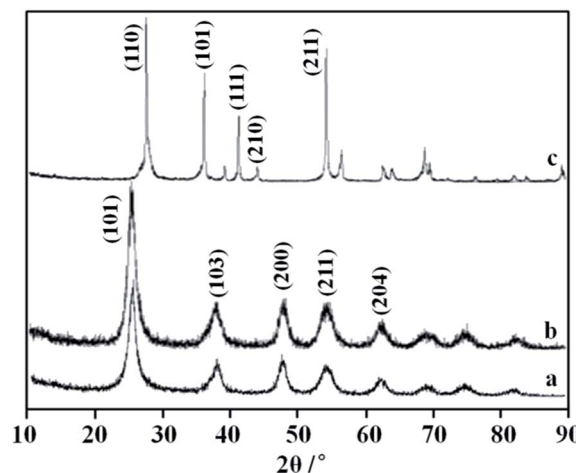

Fig. 1 XRD pattern of nano-TiO_2 after treatment in vacuum ((a) original anatase, (b) 400 °C × 40 min, (c) 1000 °C × 40 min).

about 8.30 nm. The structure of nano-TiO_2 is transferred to the structure of rutile after heat treatment in vacuum at 1000 °C, with the grain size being about 50 nm. Compared with the general heat treatment process not in vacuum, where the grain sizes of nano-TiO_2 after heat treatment in box-type furnace at 400 °C and 1000 °C are 12.6 nm and 63.7 nm respectively, under the same temperature condition the growth tendency of grain can be decreased with the heat treatment in vacuum.

The TEM pictures of nano-TiO_2 samples after heat treatment in vacuum under 400 °C and 1000 °C are shown in Fig. 2(b) and (c), respectively. It indicates that the TiO_2 nanoparticles after heat treatment in vacuum at 400 °C consist of particles with grain size of 10 nm and the particles treated at 1000 °C have a grain size of 50 nm. Both nanoparticles heat treated in vacuum are nearly spherical and homogenous.

The main text of the article should appear here with head-ings as appropriate.

The HRTEM pictures of nano-TiO_2 samples after heat treat-ment in vacuum at 400 °C and 1000 °C are shown in Fig. 3(a) and (b) respectively. The diffraction spots after Fourier trans-formation at 400 °C and 1000 °C are shown in the bottom right corner of Fig. 3(a) and (b) respectively. The results in Fig. 3 have been listed in Table 1.

The comparison between the experimental data and the theoretical values of anatase TiO_2, which can be seen from Table 1, shows that the experimental results basically agree with theoretical values. Combined with XRD analysis, one can see that the samples after heat treatment in vacuum at 400 °C are anatase TiO_2, in which the crystal face involved in the experi-ment is (002) facet and (101) facet, respectively. Note that the anatase type TiO_2 has tetragonal crystal structure, according to the formula of the interplanar spacing of tetragonal system in crystal, namely,

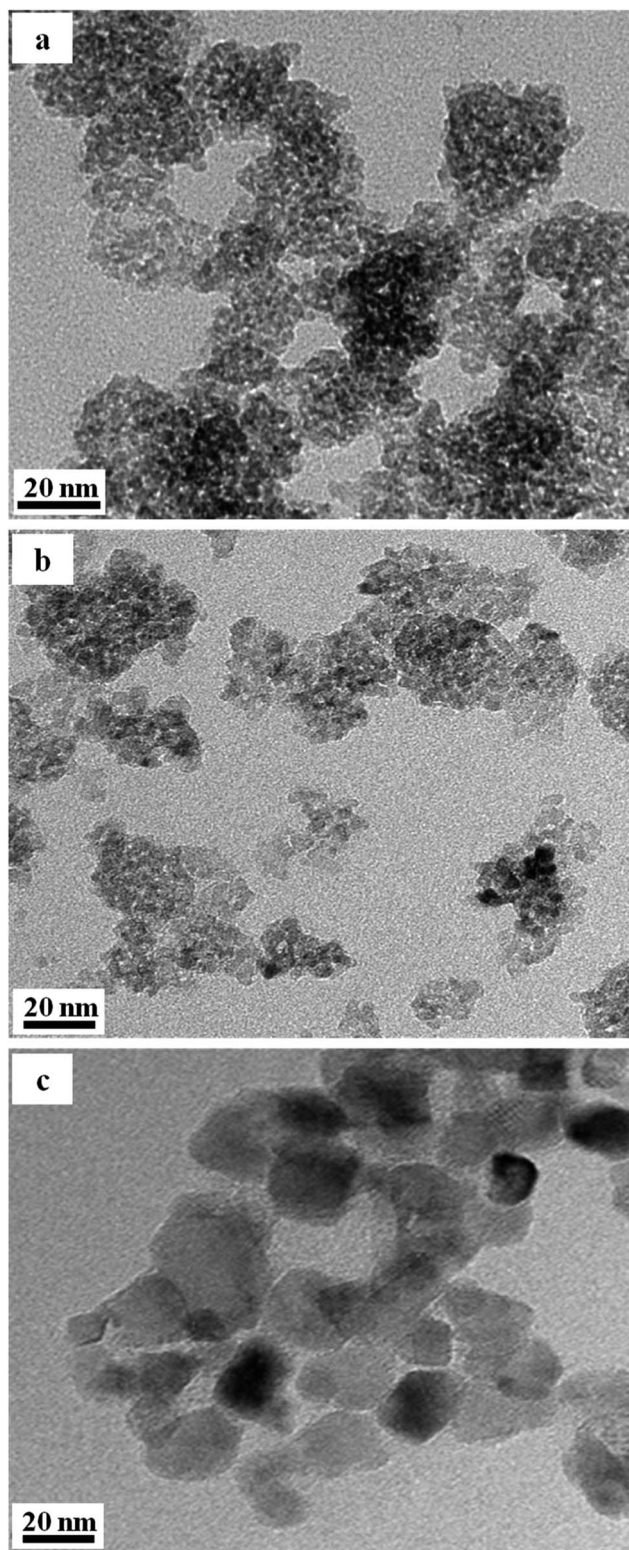$$\frac{1}{d^2} = \frac{h^2 + k^2}{a^2} + \frac{l^2}{c^2} \tag{1}$$

Fig. 2   TEM pictures of sample treated in vacuum ((a) original anatase, (b) 400 °C × 40 min, (c) 1000 °C × 40 min).

Fig. 3   HRTEM pictures of sample treated in vacuum ((a) 400 °C × 40 min, (b) 1000 °C × 40 min).

the lattice constant ratio c/a can be calculated by the two sets of interplanar spacing (d) and the corresponding crystal index (hkl). Using the d and (hkl) listed in Table 1, the lattice constant
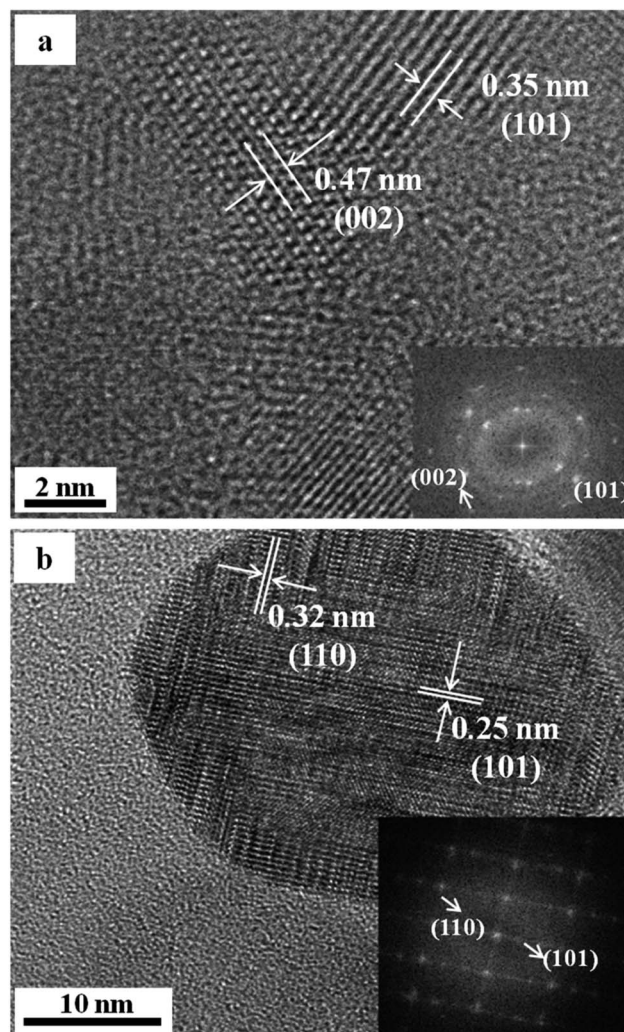
ratio of the samples after heat treatment in vacuum at 400 °C was obtained as $c/a = 2.4864$. While the lattice constant ratio of anatase nano-TiO$_2$ heat treated in a box-type furnace (non-vacuum) at 400 °C is 2.5072, with $c = 9.49749$ and $a = 3.78811$. Thus, the c/a of the samples after heat treatment in vacuum decreased by 0.829% compared with that of the samples heat treated not in vacuum at the same temperature. Similarly, it can be calculated that the lattice constant ratio of the samples after heat treatment in vacuum at 1000 °C is $=0.6414$, which decreased by 0.419% by comparing with that of the samples not in vacuum at 1000 °C. The decrease of c/a may be due to the decrease of the lattice constant c resulting from the formed during the vacuum heat treatment. The oxygen vacancies were formed owing to the diffusion of the oxygen atoms in the lattice of nano-TiO$_2$ into the vacuum atmosphere.

Analysis of X-ray photoelectron spectroscopy (XPS)

The composition of the surface element was obtained by full-spectrum scanning on the nano-TiO$_2$ samples before and after

**Table 1** Information about the crystal structure of samples treated in vacuum

	d_1 (Å)	d_2 (Å)	Ratio (d_1/d_2)	Angle (°)	Temperature (°C)
Measured values	4.69	3.5	1.34	68.7	
Anatase TiO$_2$ (hkl)	4.75 (002)	3.51 (101)	1.35	68.3	400
Measured values	3.25	2.485	1.308	90	
Rutile TiO$_2$ (hkl)	3.248 (110)	2.487 (101)	1.306	90	1000

heat treatment in vacuum. The XPS spectrum results are represented in Fig. 4. It can be seen from Fig. 4 that the elements Ti and O are mainly contained in the nano-TiO$_2$ samples before and after heat treatment in vacuum, as well as some small amounts of elements N and C. The atomic percentage of O 1s and Ti 2P of raw TiO$_2$ and heat treated TiO$_2$ in vacuum is listed in Table 2. The results show that the atomic ratio of O/Ti is less than 2 after the heat treatment in vacuum, which confirms that oxygen vacancies were formed in the lattice as the oxygen atoms in the lattice of TiO$_2$ diffuse to the vacuum. Furthermore, the intensity of the peak located at the binding energy of 531.1 eV are increased obviously for the TiO$_2$ samples after heat treatment in vacuum, indicating that the content of O^{2-} ions in the oxygen-deficient regions were increased.[20] The result also demonstrate that the oxygen vacancies were formed in the TiO$_2$ matrix after heat treatment in vacuum.

Table 2 Atomic percentage and ratio of elements O and Ti

	O 1s	Ti 2P	O/Ti
Original anatase TiO$_2$	54.12	27.06	2
TiO$_2$ modified at 400 °C	49.077	25.38	1.9337
TiO$_2$ modified at 1000 °C	32.227	16.62	1.9390

To further study the chemical valence of element Ti, the Ti 2p of the samples before and after heat treatment in vacuum was scanned in narrow zone. The XPS spectrum result is represented in Fig. 5. In the XPS database, for Ti^{4+} ions the binding energies corresponding to the photoelectron spectrums of Ti 2p$_{1/2}$ and Ti 2p$_{3/2}$ are 464.5 eV and 458.8 eV, respectively. For the compounds of Ti in different valence state, there is no change in the values of binding energy of Ti 2p$_{1/2}$, while the values of binding energy of Ti 2p$_{3/2}$ are different. For example, the binding energy values corresponding to the Ti 2p$_{3/2}$ lines of TiO$_{1.5}$, TiO, and Ti are 456.1 eV, 455.1 eV, and 454 eV, respectively.[40] It thus can be concluded that the lower the chemical valence of Ti ions, the smaller the binding energy of corresponding Ti 2p$_{3/2}$ lines. From Fig. 5 we see that the binding energy value of Ti 2p$_{3/2}$ lines of nano-TiO$_2$ before heat treatment in vacuum is 459.01 eV. The binding energy values of Ti 2p$_{3/2}$ lines of nano-TiO$_2$ after heat treatment in vacuum at 400 °C and 1000 °C are reduced to 457.6 eV and 458.2 eV, respectively. The decrease in binding energy indicates that the chemical valence of some atoms Ti in
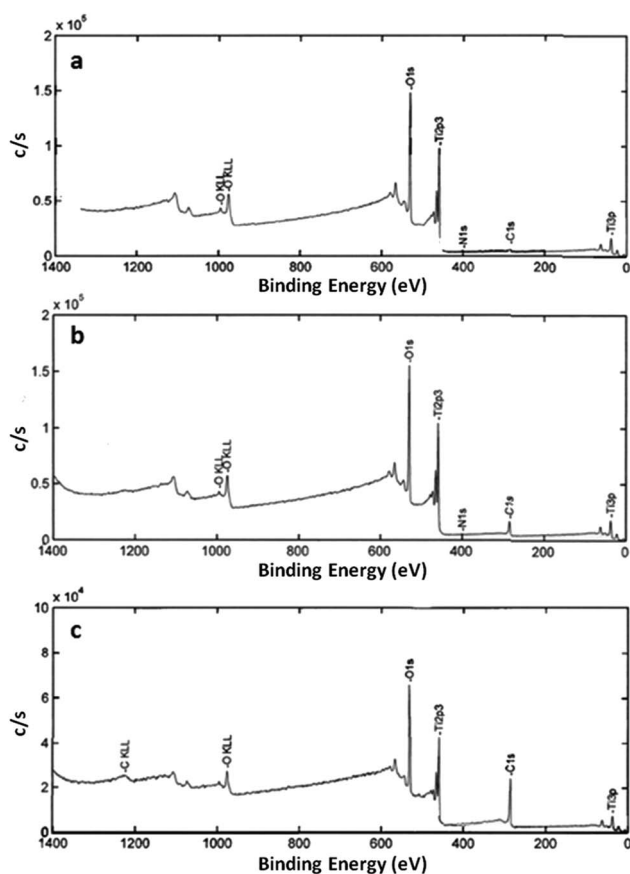
Fig. 4 XPS spectra for nano-TiO$_2$ before and after treatment in vacuum ((a) raw anatase, (b) 400 °C × 40 min, (c) 1000 °C × 40 min).
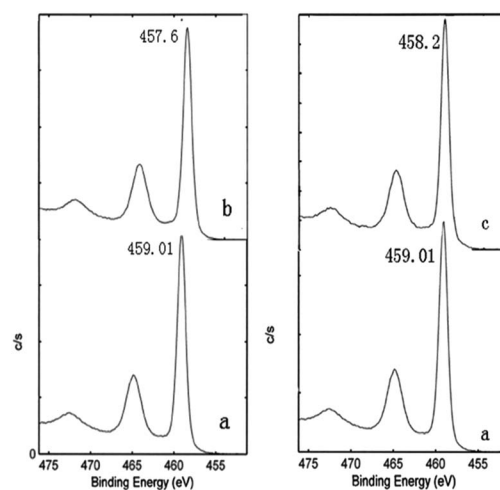
Fig. 5 XPS spectra of Ti 2p for nano-TiO$_2$ before and after treatment in vacuum ((a) raw anatase TiO$_2$, (b) 400 °C, (c) 1000 °C).

the modified samples has been changed, and there exist the Ti^{3+} ions.

Analysis of ultraviolet-visible diffuse reflectance absorption spectrum

The diffuse reflectance absorption spectrum results of nano-TiO_2 powders before and after heat treatment in vacuum are represented in Fig. 6. From Fig. 6 we see that the light region of the absorption of the nano-TiO_2 powders before heat treatment in vacuum is limited to the ultraviolet region (10–400 nm). On the contrary, the nano-TiO_2 powders after the heat treatment in vacuum is extended to the visible light region. Specifically, after heat treatment in vacuum the optical absorption threshold wavelength of the samples modified at 400 °C was shifted to 480 nm, and that modified at 1000 °C was shifted to 600 nm, indicating that the wavelengths of light the nano-TiO_2 absorbs was shifted to the visible portion (380–780 nm) of the spectrum after heat treatment in vacuum.

The effect of heat treatment in vacuum on photocatalytic activity of nano-TiO_2 under visible light

The relationship between the time and the degradation rate of methyl orange solution degraded by samples before and after heat treatment in vacuum is shown in Fig. 7(a). It can be seen from Fig. 7(a) that the nano-TiO_2 after heat treatment in vacuum has photocatalytic activity under visible light. Besides, the nano-TiO_2 powders treated at 400 °C exhibited the best photocatalytic activity under visible light. The degradation rate of nano-TiO_2 powders treated at 400 °C after 3 h of light reaches 81.233%, the degradation rate of the samples heat treated in vacuum at 1000 °C is only 40.055% after 3 h of light. This is likely related to particle size and crystal structural difference.

The photocatalytic data was future analyzed by the first-order kinetic model. As shown in Fig. 7(b), the first-order kinetic model fitted well with experimental data. The values of rate constant (k_e) and regression coefficients (R^2) were listed in Table 3. The values of R^2 were all higher than 0.900, which indicated the
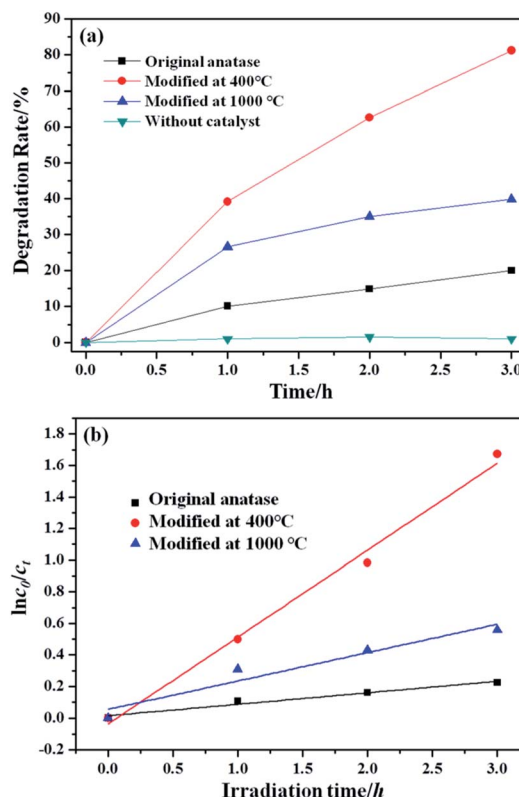
Fig. 7 (a) Degradation rate of samples before and after heat treatment in vacuum; (b) photocatalytic degradation kinetics of MO.

photocatalytic degradation reaction was in accorded with first-order kinetic. The TiO_2 treated at 400 °C had the highest k_e, where the value of 0.550 h^{-1} was acquired.

Formation mechanism of non-stoichiometric compound TiO_{2-x}

Both the HRTEM analysis and XPS analysis show that the oxygen vacancy defects were introduced into the lattice of nano-TiO_2 after heat treatment in vacuum. The atomic ratios of O/Ti in samples modified at 400 °C and 1000 °C, respectively, were 1.9337 and 1.9390, implying that the non-stoichiometric compound TiO_{2-x} was formed. This section focuses on the mechanism of the formation of the non-stoichiometric compound TiO_{2-x}.

By the non-stoichiometric compound, it refers to the compound in which the proportion between the negative ions and positive ions is not constant. Such non-stoichiometric compound can be considered as a solid solution of a high-valence compound and a low-valence compound, it could also
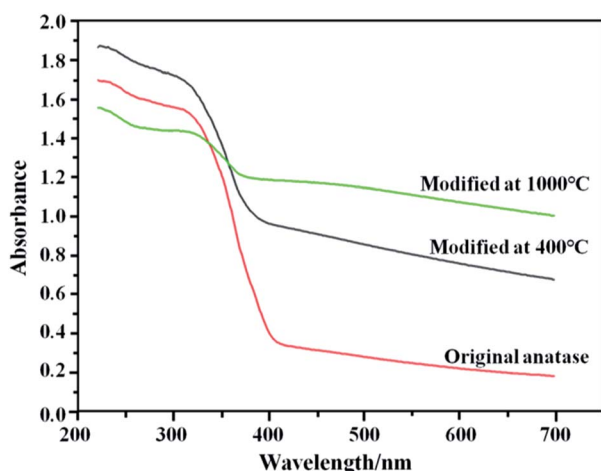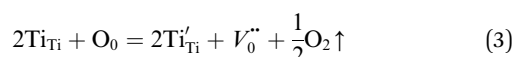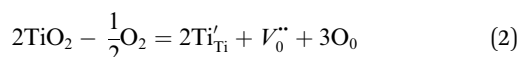
Fig. 6 UV-Vis diffusive reflectance absorption spectra of samples before and after treatment in vacuum.

Table 3 Parameters of the photocatalytic degradation kinetics

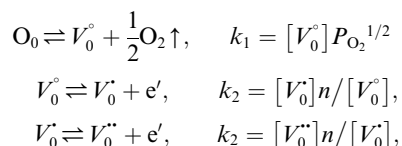| Catalysts	k_e (h^{-1})	R^2
Anatase	0.073	0.964
Modified at 400 °C	0.550	0.989
Modified at 1000 °C	0.180	0.912

be considered as a point defect.[41] In general, the formation of non-stoichiometric compounds is related to the atmosphere, pressure, and temperature. During the heat treatment in vacuum, not only the oxygen adsorbed on the surface of TiO$_2$ was desorbed but also the oxygen atoms in the lattice of TiO$_2$ diffused to the vacuum due to the lack of oxygen in the environment, leading to the formation of the oxygen vacancies and some Ti^{4+} ions were reduced to Ti^{3+} ions to keep the electric neutrality. The narrow scanning on element Ti also confirms the formation of Ti^{3+} ions. The specific reaction of the formation of TiO$_{2-x}$ can be expressed as follows. Note that in oxygen-free environments, the reaction of TiO$_2$ is:

$$2TiO_2 - \frac{1}{2}O_2 = 2Ti'_{Ti} + V_0^{\cdot\cdot} + 3O_0 \tag{2}$$

$$2Ti_{Ti} + O_0 = 2Ti'_{Ti} + V_0^{\cdot\cdot} + \frac{1}{2}O_2\uparrow \tag{3}$$

Since $Ti'_{Ti} = Ti_{Ti} + e'$, we then derive from (2) and (3) that

$$O_0 = 2e' + V_0^{\cdot\cdot} + \frac{1}{2}O_2\uparrow \tag{4}$$
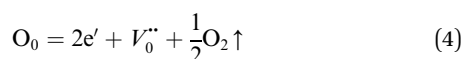
This defect reaction can be divided into the following types:

$$O_0 \rightleftharpoons V_0^{\circ} + \frac{1}{2}O_2\uparrow, \qquad k_1 = [V_0^{\circ}]P_{O_2}^{1/2}$$
$$V_0^{\circ} \rightleftharpoons V_0^{\cdot} + e', \qquad k_2 = [V_0^{\cdot}]n/[V_0^{\circ}],$$
$$V_0^{\cdot} \rightleftharpoons V_0^{\cdot\cdot} + e', \qquad k_2 = [V_0^{\cdot\cdot}]n/[V_0^{\cdot}],$$

where $n = [V_0^{\cdot}] - 2[V_0^{\cdot\cdot}]$ denotes the condition of electrical neutrality.

Case 1: suppose that $V_0^{\circ} \gg V_0^{\cdot} + [V_0^{\cdot\cdot}]$, it then holds that $V_0^{\circ} = k_1 P_{O_2}^{-1/2}$;

Case 2: suppose that $V_0^{\cdot} \rightleftharpoons V_0^{\circ} + [V_0^{\cdot\cdot}]$, then the condition of electrical neutrality is approximately equal to $n = [V_0^{\cdot}]$, and further, it holds that $n = [V_0^{\cdot}] = (k_1k_2)^{1/2}P_{O_2}^{-1/4}$;

Case 3: suppose that $V_0^{\cdot\cdot} \gg V_0^{\circ} + [V_0^{\cdot}]$, then the condition of electrical neutrality is approximately equal to $n = 2[V_0^{\cdot\cdot}]$, and further, it holds that $[V_0^{\cdot\cdot}] = \left(\frac{1}{4}k_1k_2k_3\right)^{1/3}P_{O_2}^{-1/6}$.

It is worth mentioning that the oxygen partial pressure is relatively low and the corresponding is relatively large under the heat treatment in vacuum. As a result, defect reaction belongs to the third case. Hence, the concentration of the oxygen vacancy is inversely proportional to the power of the oxygen partial pressure.

The mechanism of the effect of oxygen vacancy defects on the application of nano-TiO$_2$ under visible light.

The oxygen vacancies of the anatase nano-TiO$_2$ obtained by the heat treatment in vacuum are positively charged, and two electrons are bounded nearly to the oxygen vacancy. The two electrons are different from the general free electrons in that they are quasi-free electrons bounded by the oxygen vacancies. If they associated with the Ti^{4+} nearby, this kind of electrons would make Ti^{4+} ions into Ti^{3+} ions. If in an electric field, this kind of electron may migrate from one Ti^{4+} ion to another Ti^{4+}

ion nearby such that electronic conductivity is formed. The material with such a defect is called a n-type semiconductor. This kind of negative-ion vacancy together with the surrounding bounded excess electrons is called the color structure, in the center of which the electrons can absorb light of a certain wavelength, as illustrated in Fig. 8.

In the existing work, the introduction of the oxygen vacancy defects to the crystal structure of nano-TiO$_2$ is mainly by nonmetallic elements doping. By introducing the oxygen vacancy to the crystal structure of TiO$_2$, the non-metallic elements then can substitute the oxygen vacancy, such that TiO$_{2-x}$A$_x$ (A denotes the nonmetallic element) crystal is formed. In this case, the band gap of the nonmetallic elements doped TiO$_2$ is narrow and an obvious redshift of the threshold of optical absorption will occur. The obvious redshift then results in extended the response range of absorbed light.

In this work, the oxygen vacancies formed in the crystal structure of TiO$_2$ do not introduce other elements into the lattice of TiO$_2$. In regard to the existence of oxygen vacancies in the band structure of TiO$_2$, some scholars have measured the energy of the electron detaching from the oxygen vacancy in TiO$_2$. They claimed that the energy value is between 0.75 and 1.8 eV,[42] and the oxygen vacancy of anatase TiO$_2$ is located at 2.02–2.45 eV above the valence band. In addition, the isolated oxygen vacancy in the band structure of TiO$_2$ is between the valence band and conduction band, as can be seen from Fig. 9. Generally, photoexcitation process in light is only one step. However, for the TiO$_2$ with oxygen vacancy, the oxygen vacancy
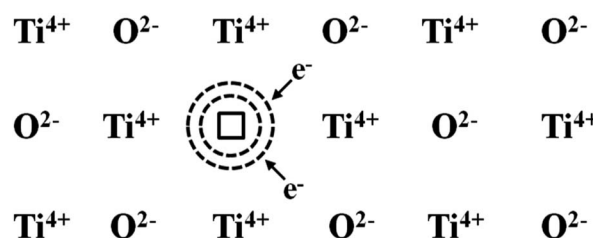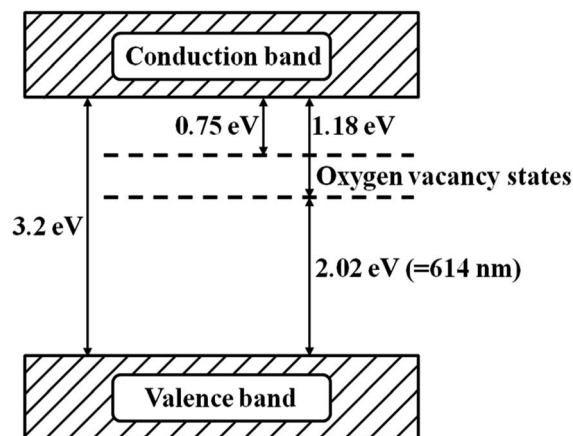

Fig. 8 Defect structure of TiO$_{2-x}$.

Fig. 9 The band structure model for the anatase TiO$_2$ with oxygen vacancies.

state would be involved in a new photoexcitation process in light. That is, the electrons on the valence band are excited with the low energy provided by visible light. The excited electrons jump to the oxygen vacant state and then to the conduction band of TiO_2 such that the visible light is absorbed.

Conclusions

(1) The oxygen vacancy and Ti^{3+} were formed in the crystal structure of nano-TiO_2 after heat treatment in vacuum, in which the oxygen vacancy located between the valence band and the conduction band of the energy band structure of nano-TiO_2. This makes the photo-generated electrons first jump into the state of oxygen vacancy under the effect of lower energy and then to the conduction band, such that the visible-light absorption is improved.

(2) The nano-TiO_2 samples can absorb the visible light of certain wavelength after heat treatment in vacuum. The wavelengths of light the nano-TiO_2 absorbs is shifted to the visible portion of the spectrum. Specifically, the optical absorption threshold wavelength of the samples modified at 400 °C and 1000 °C were shifted to 480 nm and 600 nm, respectively, after the heat treatment in vacuum.

(3) The modified samples possess visible light catalytic activity, and the degradation rate of the powders after heat treatment in vacuum at 400 °C is 81.233% after 3 hour light exposure.

Conflicts of interest

There are no conflicts to declare.

Acknowledgements

Notes and references

1 A. Fujishima and K. Honda, *J. Nat.*, 1972, **238**, 37.
2 I. Ali, M. Suhail, Z. A. Alothman and A. Alwarthan, *RSC Adv.*, 2018, **8**, 30125.
3 Y.-W. Su, W.-H. Lin, Y.-J. Hsu and K.-H. Wei, *Small*, 2014, **10**, 4427.
4 Y.-H. Chiu and Y.-J. Hsu, *Nano Energy*, 2017, **31**, 286.
5 P.-Y. Hsieh, Y.-H. Chiu, T.-H. Lai, M.-J. Fang, Y.-T. Wang and Y.-J. Hsu, *ACS Appl. Mater. Interfaces*, 2019, **11**, 3006.
6 Y.-H. Chiu, T.-H. Lai, C.-Y. Chen, P.-Y. Hsieh, K. Ozasa, M. Niinomi, K. Okada, T.-F. M. Chang, N. Matsushita, M. Sone and Y.-J. Hsu, *ACS Appl. Mater. Interfaces*, 2018, **10**, 22997.
7 Y.-S. Chang, M. Choi, M. Baek, P.-Y. Hsieh, K. Yong and Y.-J. Hsu, *Appl. Catal., B*, 2018, **225**, 379.
8 Y.-C. Pu, Y. Ling, K-D. Chang, C.-M. Liu, J. Z. Zhang, Y.-J. Hsu and Y. Li, *J. Phys. Chem. C*, 2014, **118**, 15086.
9 Y.-C. Pu, G. Wang, K.-D. Chang, Y. Ling, Y.-K. Lin, B. C. Fitzmorris, C.-M. Liu, X. Lu, Y. Tong, J. Z. Zhang, Y.-J. Hsu and Y. Li, *Nano Lett.*, 2013, **13**, 3817.
10 A. A. Valeeva, I. B. Dorosheva, E. A. Kozlova, R. V. Kamalov, A. S. Vokhmintsev, D. S. Selishchev, A. A. Saraev, E. Y. Gerasimov, I. A. Weinstein and A. A. Rempel, *J. Alloys Compd.*, 2019, **796**, 293.
11 R. Huang, S. Zhang, J. Ding, Y. Meng, Q. Zhong, D. Kong and C. Gu, *J. Colloid Interface Sci.*, 2019, **553**, 647.
12 Y.-H. Chiu, T.-F. M. Chang, C.-Y. Chen, M. Sone and Y.-J. Hsu, *Catalysts*, 2019, **9**, 430.
13 J.-B. Chemin, S. Bulou, K. Baba, C. Fontaine, T. Sindzingre, N. D. Boscher and P. Choquet, *Sci. Rep.*, 2018, **8**, 9603.
14 G. Chen, S. Ouyang, Y. Deng, M. Chen, Y. Zhao, W. Zou and Q. Zhao, *RSC Adv.*, 2019, **9**, 18652.
15 X. Shen, F. Zhang, K. Li, C. Qin, P. Ma, L. Dai and K. Cai, *Mater. Des.*, 2016, **92**, 1007.
16 Z. Yuan, S. Huang, S. Lan, H. Xiong, B. Tao, Y. Ding, Y. Liu, P. Liu and K. Cai, *J. Mater. Chem. B*, 2018, **6**, 8090.
17 L. Sutrisno, Y. Hu, X. Shen, M. Li, Z. Luo, L. Dai, S. Wang, J. L. Zhong and K. Cai, *Mater. Sci. Eng., C*, 2018, **89**, 95.
18 B. Tao, Y. Deng, L. Song, W. Ma, Y. Qian, C. Lin, Z. Yuan, L. Lu, M. Chen, X. Yang and K. Cai, *Colloids Surf., B*, 2019, **177**, 242.
19 J.-M. Li, C.-W. Tsao, M.-J. Fang, C.-C. Chen, C.-W. Liu and Y.-J. Hsu, *ACS Appl. Nano Mater.*, 2018, **1**, 6843.
20 J.-M. Li, Y.-T. Wang and Y.-J. Hsu, *Electrochim. Acta*, 2018, **267**, 141.
21 M. Samiee and J. Luo, *Mater. Lett.*, 2013, **98**, 205.
22 H. Yamashita, M. Harada, J. Misaka, M. Takeuchi, B. Neppolian and M. Anpo, *Catal. Today*, 2003, **84**, 191.
23 S. Sato, R. Nakamura and S. Abe, *Appl. Catal., A*, 2005, **284**, 131.
24 D. Li, H. Haneda, S. Hishita, N. Ohashi and N. K. Labhsetwar, *J. Fluorine Chem.*, 2005, **126**, 69.
25 D. Li, H. Haneda, N. K. Labhsetwar, S. Hishita and N. Ohashi, *Chem. Phys. Lett.*, 2005, **401**, 579.
26 J. Zhang, L. J. Xu, Z. Q. Zhu and Q. J. Liu, *Mater. Res. Bull.*, 2015, **70**, 358.
27 D. R. Zhang, H. L. Liu, S. Y. Han and W. X. Piao, *J. Ind. Eng. Chem.*, 2013, **19**, 1838.
28 W. H. Cheng, C. D. Li, X. Ma, L. M. Yu and G. Y. Liu, *Mater. Des.*, 2017, **126**, 155.
29 Y. Q. Zhang and P. J. Li, *Mater. Des.*, 2015, **88**, 1250.
30 V. Subramanian, E. Wolf and P. V. Kamat, *J. Phys. Chem. B*, 2001, **105**, 11439.
31 Y. X. Zhang, H. Ma, M. Yi, Z. G. Shen, X. Z. Yu and X. J. Zhang, *Mater. Des.*, 2017, **125**, 94.
32 G. L. Zhao, H. Kozuka and T. Yoko, *J. Ceram. Soc. Jpn.*, 1996, **104**, 164.
33 G. Colon, M. C. Hidalgo, G. Munuera, I. Ferino, M. G. Cutrufello and J. A. Navío, *Appl. Catal., B*, 2006, **63**, 45.

34 G. Colon, M. C. Hidalgo and J. A. Navio, *Appl. Catal., B*, 2009, **90**, 633.

35 L. L. Lai, W. Wen, B. Fu, X. Y. Qian, J. B. Liu and J. M. Wu, *Mater. Des.*, 2016, **108**, 581.

36 R. Asahi, T. Morikawa, T. Ohwaki, K. Aoki and Y. Taga, *Science*, 2001, **293**, 269.

37 R. Saravanan, D. Manoj, J. Qin, M. Naushad, F. Gracia, A. F. Lee, M. M. Khan and M. A. Gracia-Pinilla, *Process Saf. Environ. Prot.*, 2018, **120**, 339.

38 L. Lu, R. Shan, Y. Shi, S. Wang and H. Yuan, *Chemosphere*, 2019, **222**, 391.

39 X. Yuan, X. Wu, Z. Feng, W. Jia, X. Zheng and C. Li, *Catalysts*, 2019, **9**, 624.

40 W. J. Yin, B. Wen, C. Zhou, A. Selloni and L. M. Liu, *Surf. Sci. Rep.*, 2018, **73**, 58.

41 L. M. Zhang, X. H. Huang and X. L. Song, *Materials science foundation*, Wuhan University Press, Wuhan, 2004, p. 155.

42 D. C. Cronemeyer, *Phys. Rev.*, 1959, **113**, 1222.